Pergamon

Int. J. Solids Structures Vol. 32, No. 17/18, pp. 2657–2675, 1995

0020-7683/95 $9.50 + .00

0020-7683(94)00288-6

INTERLAMINAR DYNAMIC CRACK PROPAGATION

T. NAKAMURA, A. KUSHNER and C. Y. LO
Department of Mechanical Engineering, State University of New York at Stony Brook, NY 11794, U.S.A.

(*Received* 3 *February* 1994)

Abstract—Effective computational procedures are established and used to characterize dynamic crack propagation along material interfaces between isotropic and orthotropic materials. We first simulate a dynamic fracture experiment in which crack propagation occurs along an interface between PMMA and steel in a dynamically loaded bend specimen. In the analysis, the dynamic energy release rate and mixed-mode stress intensity factors are extracted from finite element field solutions using suitably formulated conservation integrals. These variables form the basis for defining an interface fracture criterion under dynamic conditions. In order to propagate the crack according to such a criterion, an iterative procedure is utilized to determine the correct crack tip velocity history. An important computed result, which is consistent with experimental observation, is that the energy release rate decreases as the crack propagation accelerates. The physical interpretation of this result is that less energy is absorbed by the moving crack as its velocity increases. In the second part of our study, the computational procedures are modified for the dynamic fracture analysis of a thin composite panel consisting of differently oriented orthotropic laminae. Here we investigate the interplay between delamination and buckling of the more complex structure. It is assumed that the panel contains an initial finite interlaminar crack and is subjected to a uniaxial compressive load. Without any crack extension, two buckling modes are observed under quasi-static conditions. One is characterized by an overall panel buckling and the other is dominated by a local ligament buckling near the crack. Coupling of the two modes produces not only a lower critical buckling load but also an unstable post-buckling behavior. Therefore, an embedded delamination is seen to create imperfection sensitivity, leading to limit load type behavior. Such a condition is potentially troublesome for compression loaded thin composite panels. In addition, the large compressive load may also trigger a dynamic propagation of the embedded delamination. We have simulated this unstable dynamic crack growth using the iterative method and a simplified delamination criterion. In the simulation, the energy release rate, the mixed-mode stress intensity factors and the resulting crack tip speed are obtained. These results predict that an existing embedded delamination can weaken and significantly alter the post-buckling behavior of composite panel.

1. INTRODUCTION

The dynamic fracture mechanics study of bimaterial interfaces is still limited. There are some analytical studies by Willis (1971), Wu (1991) and Liu *et al.* (1993) and some experimental investigations by Tippur and Rosakis (1991) and Lambros and Rosakis (1995). In our previous paper (Lo *et al.*, 1994), new computational procedures were presented and used for the analysis of dynamic interface cracks between two isotropic materials. Using the new iterative procedure and an assumed fracture toughness, it was demonstrated that a simulation of crack propagation can be carried out without prior knowledge of the history of crack tip speed. Essentially, the iterative procedure determines an instantaneous crack tip speed which yields equilibrium between the crack driving force (or available $\mathcal{G}$) and the dynamic interface resistance (or material's $\mathcal{G}_D$). The computed results were compared with the limited experimental data available from Tippur and Rosakis (1991). In addition, an accurate method was introduced to separate the dynamic mixed-mode stress intensity factors using the interaction integral.

In this paper, the computational procedures are extended and applied in two analyses. First, in view of the more detailed experimental study by Lambros and Rosakis (1995), the previously proposed interface fracture criterion is reformulated and a closer inspection of the dynamic fracture behavior is carried out. Second, in order to show the effectiveness of the procedures, they are used in the analysis of a more complex structural model under large deformation conditions.

In the first analysis, the interface crack in a linear elastic polymethylmethacrylate (PMMA)–steel specimen used by Lambros and Rosakis (1995) is considered. The key features of their experimental measurements are a rapidly increasing crack tip speed reaching the wave speeds of PMMA and a decreasing toughness in terms of energy release rate for higher crack tip speeds. In order to reproduce the experiments and establish correct toughness conditions, the computational analysis is carried out with a finer mesh and a new form of the proposed toughness formula. With the computed results, we also investigate suitable parameters in the dynamic fracture criterion of the interface cracks. In the second analysis, a composite panel consisting of an orthotropic panel containing an embedded delamination is considered. The aim of this study is to determine the effect of the delamination on the overall structural strength of the panel and to show the applicability of the present procedures to an important class of structural problems.

2. DYNAMIC INTERFACE CRACK

2.1. *Asymptotic singular crack tip field*

Under dynamic conditions, the asymptotic crack tip solution is a function of the instantaneous crack tip speed. In general, the size of the crack tip region dominated by the asymptotic singular field or K-field is smaller than that of a stationary crack. This aspect and the effect of higher order terms in interface crack mechanics were recently discussed by Liu *et al.* (1993). The steady state or the singular fields close to the tip of a crack moving along the interface of two anisotropic elastic solids are given by Yang *et al.* (1991). They used Stroh's (1962) steady state formulation as a basis for deriving the solution. Their study shows that, within a K-dominated zone, the crack tip field consists of a coupled in-plane oscillatory field characterized by a complex stress intensity factor and a non-oscillatory out-of-plane field characterized by a real stress intensity factor. The latter field corresponds to the mode III deformation and is not accounted for here.

The asymptotic field of the dynamic interface crack can be conveniently characterized by the compliance-like hermitian matrix $\mathbf{H}$. Directing attention to the in-plane deformation of a crack moving along the interface of two different orthotropic solids with a crack tip velocity v, the matrix $\mathbf{H}$ can be reduced to the following 2×2 complex variable matrix:

$$\mathbf{H} = \begin{bmatrix} \dfrac{\kappa_{22}^1\zeta_1^2\sqrt{[2(1+s_1)/\varphi_1]}}{C_{66}^1 R_1} + \dfrac{\kappa_{22}^2\zeta_2^2\sqrt{[2(1+s_2)/\varphi_2]}}{C_{66}^2 R_2} & \mathrm{i}\left(\dfrac{\kappa_{22}^1-\kappa_{12}^1\zeta_1^2/\varphi_1}{C_{66}^1 R_1} - \dfrac{\kappa_{22}^2-\kappa_{12}^2\zeta_2^2/\varphi_2}{C_{66}^2 R_2}\right) \\ -\mathrm{i}\left(\dfrac{\kappa_{22}^1-\kappa_{12}^1\zeta_1^2/\varphi_1}{C_{66}^1 R_1} - \dfrac{\kappa_{22}^2-\kappa_{12}^2\zeta_2^2/\varphi_2}{C_{66}^2 R_2}\right) & \dfrac{\kappa_{22}^1\sqrt{[2(1+s_1)\varphi_1]}}{C_{66}^1 R_1} + \dfrac{\kappa_{22}^2\sqrt{[2(1+s_2)\varphi_2]}}{C_{66}^2 R_2} \end{bmatrix}. \tag{1}$$

Here

$$\varphi_\alpha = \xi_\alpha\zeta_\alpha\sqrt{\frac{\kappa_{11}^\alpha}{\kappa_{22}^\alpha}}, \quad s_\alpha = \frac{\zeta_\alpha^2+\kappa_{11}^\alpha\kappa_{22}^\alpha\xi_\alpha^2-(1+\kappa_{12}^\alpha)^2}{2\sqrt{(\kappa_{11}^\alpha\kappa_{22}^\alpha)}\xi_\alpha\zeta_\alpha} \tag{2}$$

and $\kappa_{ij}^\alpha = C_{ij}^\alpha/C_{66}^\alpha$, $\xi_\alpha = \sqrt{[1-(\rho_\alpha v^2/C_{11}^\alpha)]}$ $\zeta_\alpha = \sqrt{[1-(\rho_\alpha v^2/C_{66}^\alpha)]}$ and ρ_α are the mass densities of materials. Also, the generalized Rayleigh wave function is $R_\alpha = \kappa_{22}^\alpha(\kappa_{22}^\alpha\varphi_\alpha - 1+\zeta_\alpha^2) - (\kappa_{12}^\alpha\zeta_\alpha)^2/\varphi_\alpha$, C_{ij}^α is the conventional 6×6 matrix notation of material constant and v is the crack tip velocity. Here α indicates materials on the left side ($\alpha = 1$) and the right side ($\alpha = 2$) of the crack propagating direction. The components of the above matrix are used to define the crack tip solution.

The asymptotic stresses within the K-dominated zone can be expressed in the following form:

$$\sigma_{ij}(r,\theta;\varepsilon)=\frac{\mathrm{Re}[\mathbf{K}r^{i\varepsilon}]}{\sqrt{(2\pi r)}}\tilde{\sigma}_{ij}^{\mathrm{I}}(\theta;\varepsilon)+\frac{\mathrm{Im}[\mathbf{K}r^{i\varepsilon}]}{\sqrt{(2\pi r)}}\tilde{\sigma}_{ij}^{\mathrm{II}}(\theta;\varepsilon), \tag{3}$$

where r, θ are polar coordinates with their origin located at the moving crack tip and $\tilde{\sigma}_{ij}^{\mathrm{I}}$ and $\tilde{\sigma}_{ij}^{\mathrm{II}}$ are dimensionless angular functions. The complex stress intensity factor is defined as $\mathbf{K}=K_{\mathrm{I}}+\mathrm{i}K_{\mathrm{II}}$. The explicit forms of these functions are given by Yang *et al.* (1991). Also, ε is the oscillatory index defined with Dundurs' parameter β as

$$\varepsilon=\frac{1}{2\pi}\ln\frac{1-\beta}{1+\beta}\quad\text{where}\quad\beta=\frac{-H_{12}}{\sqrt{(H_{11}H_{22})}}. \tag{4}$$

Here, H_{11}, H_{22} and H_{12} are components in matrix $\mathbf{H}$ [eqn (1)]. Unlike the static case, the oscillatory index ε under dynamic conditions depends not only on the material mismatch but also on the *instantaneous* crack tip velocity v. It is important to note that even for some bimaterial combinations for which $\varepsilon=0$ in the static case, ε is non-zero under dynamic conditions ($v>0$). This means the oscillatory behavior exists in the dynamic crack tip field for all bimaterial combinations except the homogeneous case. As in the static case, the unit of the stress intensity factors contains an imaginary number when $\varepsilon\neq 0$.

An important parameter in defining the fracture toughness or the critical energy release rate is the phase angle. It is essentially the ratio of the shear to normal traction ahead of the crack which varies with the distance from the tip due to the oscillatory nature of the field. Thus, the phase angle must be defined in terms of a characteristic length scale L as,

$$\psi(L)=\tan^{-1}\left\{\frac{\mathrm{Im}[\mathbf{K}L^{i\varepsilon}]}{\mathrm{Re}[\mathbf{K}L^{i\varepsilon}]}\right\}=\tan^{-1}\left\{\left(\frac{\sigma_{12}}{\eta\sigma_{22}}\right)_{r=L}\right\}. \tag{5}$$

Here η is a traction resolution factor, $\eta=\sqrt{(H_{22}/H_{11})}$. Due to this factor, the stress intensity factors defined here do not reduce to the classically defined dynamic stress intensity factors for an isotropic homogeneous material shown, for example, by Freund (1990). Since the phase angle (5) is a function of length, when the distance changes from L_1 to L_2, the difference of the two phase angles is

$$\Delta\psi=\psi(L_2)-\psi(L_1)=\varepsilon\ln\left(\frac{L_2}{L_1}\right). \tag{6}$$

In the static case, where ε is generally very small, this difference remains relatively small. However, ε can be very large in the dynamic case, especially at high crack tip speeds. Consequently $\Delta\psi$ can be quite large, and also it is not a constant for two characteristic lengths as in the static cases. Therefore, the choice of L must be made very carefully for dynamic interface cracks.

2.2. *Dynamic energy release rate*

Because the energy release rate is a physical quantity which defines an energy flow into the moving crack tip, it is always an important and fundamental parameter to characterize the dynamic fracture processes. This is true even when a well-established singular field does not exist near the crack tip. It also has an advantage in interface crack problems since any fracture criteria based solely on critical stress and displacement can be ambiguous due to the near tip oscillatory field. Based on the fundamental crack tip integral, the energy release rate $\mathscr{G}$ of an elastic two-dimensional solid under dynamic conditions with a crack moving along the x_1-direction is

$$\mathcal{G} = \lim_{\Gamma \to 0} \int_{\Gamma} \left[(W+T) n_1 - \sigma_{ij} \frac{\partial u_i}{\partial x_1} n_j \right] \mathrm{d}\Gamma, \tag{7}$$

where the integrating path Γ is an arbitrary contour surrounding a crack tip. The outward normal unit vector of Γ is denoted by n_j. Also σ_{ij} and u_i are Cartesian components of stress and displacements, respectively, W is the strain energy density and T is the kinetic energy density at a material point. The above expression expresses the instantaneous energy release rate for any crack configuration, including interface cracks in orthotropic materials, as long as the limiting process is preserved. Under a steady state crack growth condition and if the material properties are constant along the x_1-direction, the integral becomes path independent.

The fundamental crack tip integral for the energy release rate (7) is given in terms of the limiting field or the near tip quantities. Since the precise numerical evaluation of the limiting fields is difficult, an accurate procedure based on the "domain integral formulation" is adopted here. In the formulation, we use a weighting function q to transform these path integrals to area/domain integrals as,

$$\mathcal{G} = \int_A \left[\sigma_{ij} \frac{\partial u_i}{\partial x_1} \frac{\partial q}{\partial x_j} - (W+T) \frac{\partial q}{\partial x_1} + \rho \left(\frac{\partial^2 u_i}{\partial t^2} \frac{\partial u_i}{\partial x_1} - \frac{\partial u_i}{\partial t} \frac{\partial^2 u_i}{\partial x_1 \partial t} \right) q \right] \mathrm{d}A, \tag{8}$$

where A is the domain enclosed by the path Γ and crack surfaces. The weighting parameter q is a smooth function of x_1 and x_2. It has values of zero on Γ and unity at the crack tip. The domain integral expressions are implemented in post-processing programs to evaluate $\mathcal{G}$ and also I shown in the next section. In our analysis, five to six domains enclosing up to 500 elements are typically chosen to compute $\mathcal{G}$ and I. The locations of the domains must move with the crack tip as it propagates through the interface. The variations of $\mathcal{G}$ from different domains are used to check the accuracy of the solutions.

The relation between energy release rate $\mathcal{G}$ and stress intensity factors for the dynamic interface crack is given by Yang *et al.* (1991) as

$$\mathcal{G} = \frac{H_{22}}{4 \cosh^2(\pi \varepsilon)} |\mathbf{K}|^2. \tag{9}$$

In the analysis, independently computed $\mathcal{G}$ and K_{I}, K_{II} are used in the above formula to determine the consistency conditions.

2.3. *Extraction of dynamic stress intensity factors*

An accurate determination of mode mixity is important since experimental results indicate that toughness of an interface depends highly on the ratio of shear to tensile modes. Here we modify the "interaction integral" which is used in the previous paper (Lo *et al.*, 1994) for orthotropic materials. As compared with the isotropic materials, computations for an orthotropic material are significantly more difficult. The form of this integral is shown as

$$I = \lim_{\Gamma \to 0} \int_{\Gamma} \left[\left(\sigma_{ij} \varepsilon_{ij}^{\mathrm{aux}} + \rho \frac{\partial u_i}{\partial t} \frac{\partial u_i^{\mathrm{aux}}}{\partial t} \right) n_1 - \left(\sigma_{ij} \frac{\partial u_i^{\mathrm{aux}}}{\partial x_1} + \sigma_{ij}^{\mathrm{aux}} \frac{\partial u_i}{\partial x_1} \right) n_j \right] \mathrm{d}\Gamma. \tag{10}$$

Here terms with the superscript "aux" are the auxiliary functions defined from a known solution. Similar to the case of energy release rate, accurate calculation of I requires an integral over a finite domain and the above integral is reformulated as

$$I = \int_A \left[\left(\sigma_{ij} \frac{\partial u_i^{\text{aux}}}{\partial x_1} + \sigma_{ij}^{\text{aux}} \frac{\partial u_i}{\partial x_1} \right) \frac{\partial q}{\partial x_j} - \left(\sigma_{ij} \varepsilon_{ij}^{\text{aux}} + \rho \frac{\partial u_i}{\partial t} \frac{\partial u_i^{\text{aux}}}{\partial t} \right) \frac{\partial q}{\partial x_1} \right.$$

$$\left. + \rho \left(\frac{\partial^2 u_i}{\partial t^2} \frac{\partial u_i^{\text{aux}}}{\partial x_1} + \frac{\partial^2 u_i^{\text{aux}}}{\partial t^2} \frac{\partial u_i}{\partial x_1} - \frac{\partial^2 u_i}{\partial x_1 \partial t} \frac{\partial u_i^{\text{aux}}}{\partial t} - \frac{\partial u_i}{\partial t} \frac{\partial^2 u_i^{\text{aux}}}{\partial x_1 \partial t} \right) q \right] \mathrm{d}A. \quad (11)$$

For the auxiliary solution in eqn (11), we used the asymptotic solutions for a steady state interface crack given by Yang *et al.* (1991). The form for this orthotropic singular field is very complex. Using the dynamic interaction integral (11) and the relationship between the energy release rate and the dynamic stress intensity factors (9), one can effectively extract mode I and mode II stress intensity factors from the computed solution. The following equation gives the relationship between the dynamic interaction integral I and the stress intensity factors of the actual and auxiliary fields,

$$I = \frac{H_{22}}{2\cosh^2(\pi\varepsilon)} (K_{\text{I}} K_{\text{I}}^{\text{aux}} + K_{\text{II}} K_{\text{II}}^{\text{aux}}). \quad (12)$$

This is the fundamental equation which connects the computable interaction integral I shown in eqn (11) to the unknown stress intensity factors of the dynamic interface crack **K**. The idea here is to choose two suitable auxiliary fields whose complete field quantities, including $K_{\text{I}}^{\text{aux}}$ and $K_{\text{II}}^{\text{aux}}$, are known *a priori*. Then, once two interaction integrals with respective auxiliary fields are computed, the unknown K_{I} and K_{II} of the actual field can be calculated. Suitable choices for auxiliary fields are the asymptotic solutions which give either pure mode I or mode II fields. A more detailed description of the procedure for extraction of those stress intensity factors is given by Lo *et al.* (1994).

2.4. *Dynamic interface growth criteria*

It is useful to establish a criterion which characterizes the dynamic fracture resistance or toughness of an interface between two materials. A toughness formula will help focus the interpretation of experiments where interpretation of data is difficult under dynamic conditions. More importantly, such a formula is necessary in a simulation analysis to determine the influence on structural integrity of a structure with an embedded delamination.

We postulate that a criterion for crack propagation is controlled solely by the instantaneous energy release rate. We note that other criteria based on critical crack tip opening displacement (CTOD) or critical stress ahead of crack can be also adopted and implemented in the iterative procedure discussed in the next section. More detailed discussions of the choice of growth criterion are given at the end of this paper. Under a $\mathcal{G}$ controlled criterion, crack growth occurs when the driving force or available $\mathcal{G}$ is equal to the dynamic fracture toughness of the interface $\mathcal{G}_{\text{D}}$. Furthermore, we assume $\mathcal{G}_{\text{D}}$ is given as a function of the instantaneous crack tip velocity and the phase angle. Under these conditions, crack propagation is expressed as $\mathcal{G} = \mathcal{G}_{\text{D}}(v, \psi)$. Here we formulate a possible dynamic interface criterion. Requirements of a good formula are, first, it should be able to cover a wide range of interfaces under various boundary conditions. Second, it should contain a minimum number of parameters, especially those used for "fitting" with empirical data. Third, it is ideal to have a formula which can be related to physical phenomena associated with interface crack propagation.

In our previous paper, lacking sufficient experimental evidence, we proposed a formula based on a superposition of formulae for the static interface crack and the dynamic homogeneous crack. Here we propose a slightly modified formula in view of new experimental data by Lambros and Rosakis (1995). The proposed criterion is expressed as,

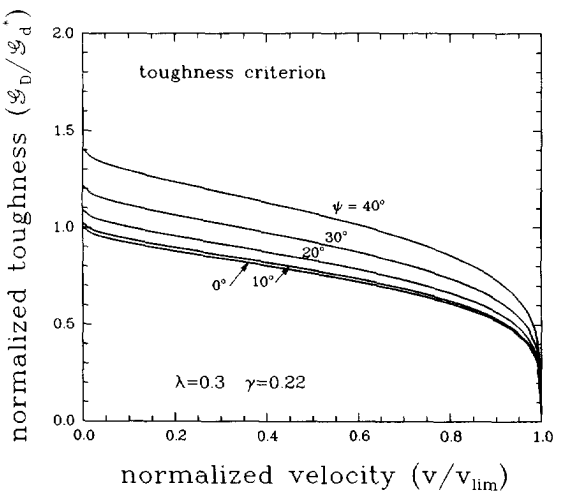

Fig. 1. Normalized fracture toughness criterion plotted as a function of crack tip velocity for various phase angles. The parameters for $\mathcal{G}_D$ in eqn (13) are $\lambda = 0.3$ and $\gamma = 0.22$.

$$\mathcal{G}_D(v, \psi; \lambda, \gamma) = \frac{\mathcal{G}_d^*[1 - \sqrt{(v/v_{lim})}]^\gamma}{1 + (\lambda - 1)\sin^2 \psi}, \tag{13}$$

where $\mathcal{G}_d^*$ can be regarded as the dynamic crack initiation toughness under $\psi = 0°$ and v_{lim} is the limiting velocity when the energy release rate becomes zero or infinite depending on the sign of γ. In addition λ and γ are the fitting parameters and suitable values are chosen for each interface. In the above formula, the denominator essentially takes into account the toughness increase under shear dominated modes and the numerator represents the relationship between the energy release rate and the crack tip speed. Other forms of the function can be developed which represent similar relationships between $\mathcal{G}_D$ and v, ψ. Lambros and Rosakis (1995) proposed a criterion based on constant CTOD. The advantage of the above function (13) is that it is simple, physically based, and has the freedom to cover a wide range of possible criteria by changing the parameters λ and γ. The effects of crack tip speed and phase angle are seen in the family of toughness curves plotted in Fig. 1. The values of parameters are the ones used in the following analysis.

3. DYNAMIC DECOHESION OF A PMMA–STEEL INTERFACE

3.1. *Computational model*

In our earlier paper (Lo *et al.*, 1994), we have simulated the dynamic fracture experiment discussed in Tippur and Rosakis (1991) for a PMMA–aluminum specimen. In the experiment, they employed the coherent grading sensing (CGS) technique to measure the deformation fields near a growing crack tip. However, their interpretation of dynamic energy release rate was incomplete and their only accurate experimental data presented was the crack tip speed history. In the computational study, a suitable dynamic crack toughness criterion was implemented in the iterative procedure and appropriate parameters were determined after comparing with the crack tip speed record. Recently, Lambros and Rosakis (1995) obtained accurate interpretation of $\mathcal{G}$ and K from the CGS measurements of a PMMA–steel specimen. Their results revealed a drastically different relationship between the dynamic interface toughness ($\mathcal{G}_D$) and the crack tip velocity (v). In view of the new experimental results, we have reformulated our dynamic interface toughness formula and carried out a more detailed inspection of the dynamic interface crack propagation behavior.

Figure 2(a) shows the PMMA–steel bimaterial specimen used in the experimental analysis of Lambros and Rosakis (1995). The thickness of the plate is 9 mm. A notch of initial length $a_0 = 25$ mm was cut through the interface after the two materials were bonded together. The specimen was loaded to fracture by means of a drop tower weight impacting

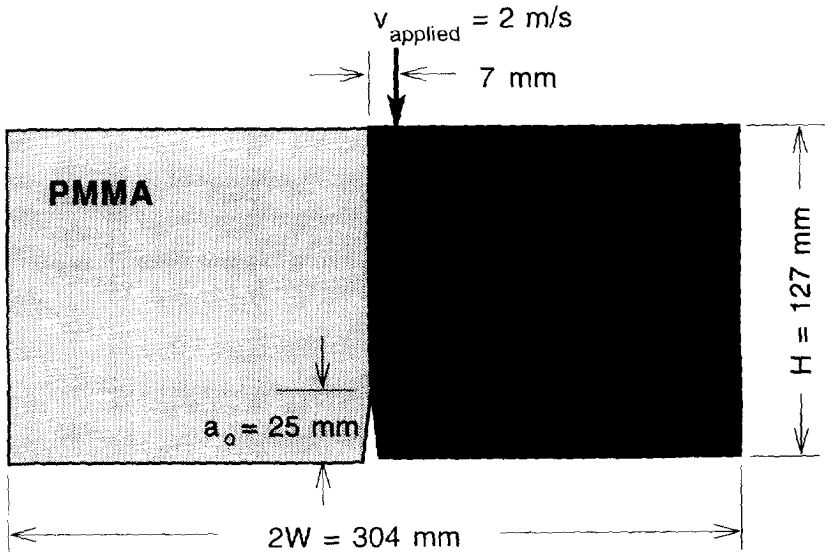

(a)

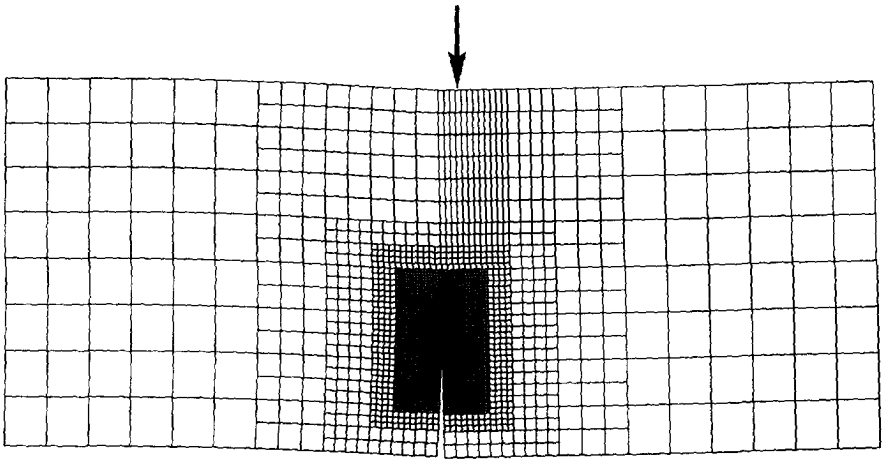

(b)

Fig. 2. (a) Schematic of the bimaterial bend specimen used by Lambros and Rosakis (1995) for the dynamic interface fracture testing. (b) Plane stress finite element model of the bend specimen.

slightly away from the mid-span of the specimen at 4 m s^{-1}. By taking into account the deformation of the drop weight, we impose a constant prescribed velocity of 2 m s^{-1} at 7 mm off the interface on the steel side. We have constructed a finer finite element mesh using 4182 plane stress four-noded elements for this analysis as shown in Fig. 2(b). The length of the elements in the vicinity of the crack is chosen to be 0.5 mm. The element sizes are increased with their distances to the crack. We used the material properties given by Lambros and Rosakis (1995). They are $E_1 = 3.24$ GPa, $\nu_1 = 0.35$, $\rho_1 = 1190$ kg m^{-3}, $c_S^1 = 1000$ m s^{-1} and $c_L^1 = 2080$ m s^{-1} for PMMA. For the steel, they are $E_2 = 208$ GPa,

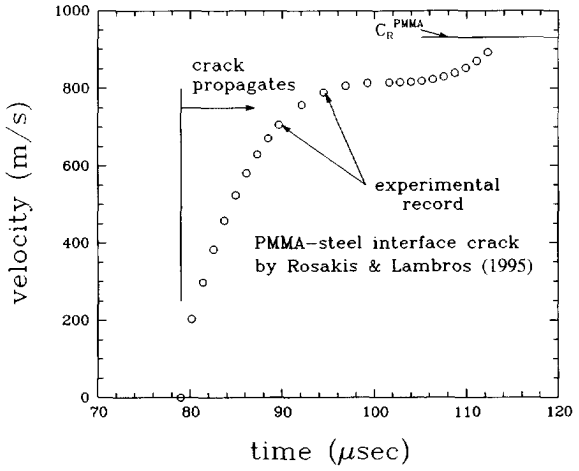

Fig. 3. The experimental measurements of crack tip velocity by Lambros and Rosakis (1995).

$\nu_2 = 0.3$, $\rho_2 = 7833$ kg m^{-3}, $c_S^2 = 3186$ m s^{-1} and $c_L^2 = 5960$ m s^{-1}. The specimen is not supported at both ends and principal loading is described by one-point-bend. The crack growth initiation occurred 79 μs after the weight impact in the experiment and we impose this elapsed time as the initiation time.

In carrying out the computational analysis, the techniques described in the previous paper are employed. To simulate physically the crack propagation by changing the crack tip boundary condition, the node release technique is employed. The advantage of this technique over other existing methods is that it requires no special type of element or remeshing. The other procedures are not suitable for the interface crack growth since the field near the tip is highly oscillatory. In addition, the iterative procedure is used for the simulation without the input of crack tip velocity. This procedure is necessary to implement a fracture criterion and essential to carry out computational analysis where no prior record of crack tip speed is available. Detailed descriptions of these procedures are given by Lo *et al.* (1994).

In order to replicate the experimental procedure, initially we have carried out the simulation with input velocity history which was measured accurately in the experiment. Figure 3 shows the record of the crack tip speed along the PMMA–steel interface obtained by Lambros and Rosakis (1995). After the initial analysis, suitable values are chosen for the parameters in the crack growth criterion (13). Using the iterative procedure, this criterion is applied in the simulation study without input crack tip velocity. In both cases, the energy release rate and the stress intensity factors are computed at every step using the integrals (8) and (11).

3.2. *Computed results*

At $t = 0$, the constant velocity 2 m s^{-1} is prescribed near the mid-span of the specimen to approximate the drop weight impact. After the impact, the compressive wave, primarily in the steel region, traverses to the crack tip region. It takes about 30 μs for sizable loading to build up in the crack tip region as shown by the dynamic energy release results in Fig. 4(a). The energy release rate continues to rise while the crack tip remains stationary, except near $t = 65$ μs where it shows the effect of a reflected wave from the boundary. At $t = 79$ μs the constraint holding the two crack tip nodes is removed and crack growth initiation is simulated. The initiation toughness is approximately 190 N m^{-1} and the phase angle is 18° [see Fig. 4(b)]. After the initiation, the crack tip velocity exactly follows the experimental record shown in Fig. 3. During each node release step, the dynamic energy release rate and the stress intensity factors are computed at every increment and the average over the step is reported as the mid-step value. Once the propagation begins, the energy release rate declines monotonically as the crack tip speed increases. More precisely, it implies that less energy is flowing into the crack tip as it increases its speed. Physically, this phenomenon

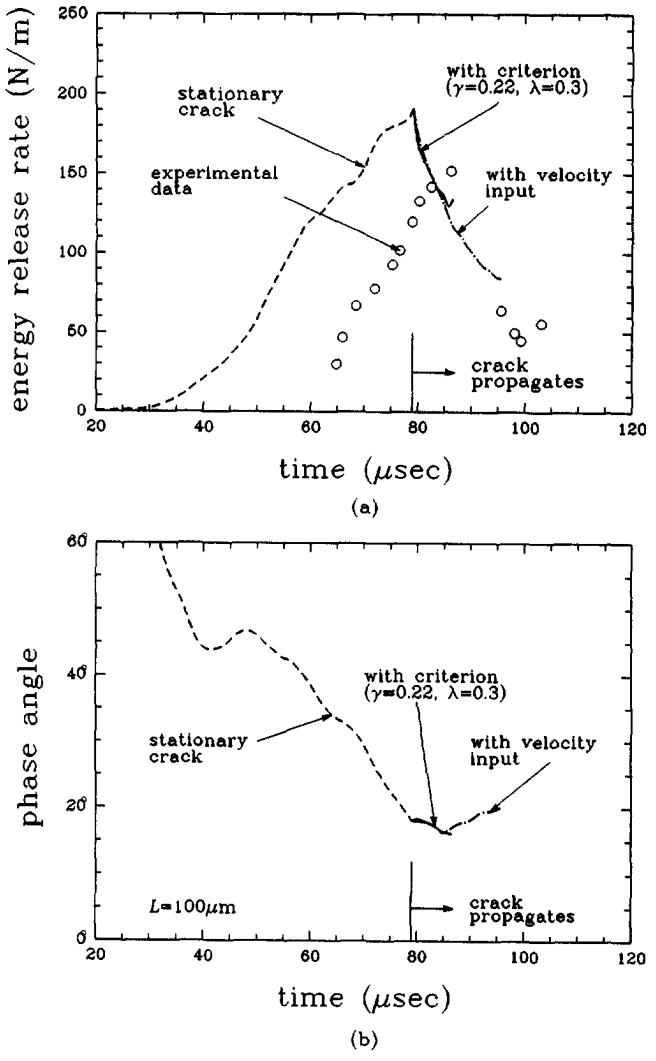

Fig. 4. (a) Energy release rate as a function of time. The dashed line is for $\mathcal{G}$ of the stationary crack. The crack initiates at $t = 79$ μs. The dynamic $\mathcal{G}$ of the propagating crack is shown for the input velocity case and the model with criterion (13). The experimental measurements by Lambros and Rosakis (1995) are also shown with circles. (b) Phase angle as a function of time. The results for a propagating crack are shown for the input velocity case and the model with criterion (13).

occurs when the acceleration of the moving crack tip is sufficiently high. For example, it has been known from earlier analytical and computational studies that the energy release rate drops suddenly when a stationary crack tip begins to propagate at a finite velocity in zero time.

The decreasing energy release rate after the initiation is consistent with the result reported by Lambros and Rosakis (1995) in their experiment. For comparison, the experimentally measured $\mathcal{G}$ is also shown in the same figure. The time lag between the computational and experimental results can be explained by the stress field measurement location chosen in the experiment. With the actual specimen, plane stress conditions hold outside the near tip three-dimensional region. Therefore, the stress field at some distance away from the crack tip must be used for the evaluation of the energy release rate. Since the wave generated at the crack tip takes a finite time to reach this location, approximately 10 μs time lag occurs in the experimental results. The slight difference in the peak values can also be attributed to wave dispersion at the measurement location and the approximate loading condition used in the computational analysis. Nevertheless, the agreement between the computed and experimental results is remarkable considering the unstable nature of

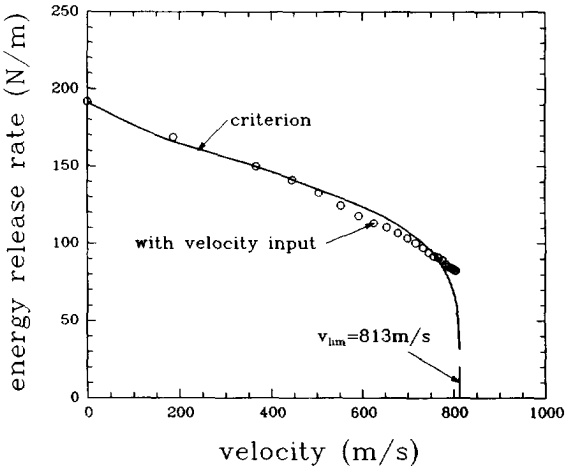

Fig. 5. Energy release rate adjusted with phase angle as a function of crack tip speed. Each circle represents the result of a node release step with input velocity case. The solid line is fracture toughness criterion (13) with $\lambda = 0.3$, $\gamma = 0.22$ and $v_{lim} = 813$ m s^{-1}.

the transient problem and the complex deformation field of interface crack. We note that this behavior contradicts the many earlier experimental results [for example, Kobayashi and Dally (1979); Ravi-Chandar and Knauss (1984); Rosakis *et al.* (1984)] observed for dynamically propagating cracks in homogeneous materials.

The results for the phase angle are shown in Fig. 4(b). In reporting the phase angle, the characteristic length is chosen to be $L = 100$ μm. The choice of an appropriate length is important in dynamic interface crack problems since the oscillatory index ε changes with v and simple translation of ψ for a different L cannot be made as in the static case. In addition, the fracture criterion (13) is greatly influenced by the value of L. In the figure, the phase angle during the early period ($t < 30$ μs) is inaccurate since there is not sufficient crack tip loading. In the stationary crack phase, the phase angle starts out with a large value, indicating a presence of large antisymmetrical or shear deformation. This condition is caused by the different wave speeds for PMMA and steel. The loading wave arrives much faster on the steel side and creates an asymmetrical condition leading to shear stress across the crack plane. The relative magnitude of shear steadily decreases as the primary loading tends to that of symmetrical structural bending, as shown by the drop of ψ. This trend reverses once the crack initiation occurs at $t = 79$ μs. The rapidly propagating crack tip generates larger asymmetrical deformation and causes the phase angle to increase. These results are consistent with the earlier results given by Lo *et al.* (1994).

Based on the input velocity results, we have attempted to determine suitable values for the parameters in the fracture criterion (13) to represent the toughness of a PMMA–steel interface. First, we preset the parameter λ for the mixed-mode influence to be $\lambda = 0.3$, which is the value suggested by Hutchinson and Suo (1991) for interface cracks. Also we note that the variation of ψ (with $L = 100$ μm) appears to be small during the propagation as shown in Fig. 4(b). In Fig. 5, the phase angle adjusted $\mathcal{G}$ is plotted as a function of the crack tip velocity. To fit with this input velocity result, we have determined the most suitable values for the parameters γ and v_{lim} in eqn (13). In the figure, the criterion (13) with $\gamma = 0.22$ and $v_{lim} = 813$ m s^{-1} is shown. In the next simulation, we demonstrate effectiveness of the proposed criterion and the iterative procedure by replicating the dynamic crack propagation without using the crack tip velocity as input.

The computation is carried out with the same initial and boundary conditions as the previous input velocity case. The only difference is the crack tip speed history since the second analysis has no prior input velocity. A slight difference in v is expected to cause some differences in $\mathcal{G}$ and ψ. The energy release rate and phase angle obtained by the fracture criterion are shown in Fig. 4. They show excellent agreement with the earlier input velocity results. Usually it takes four to five iterations for each step to determine the correct

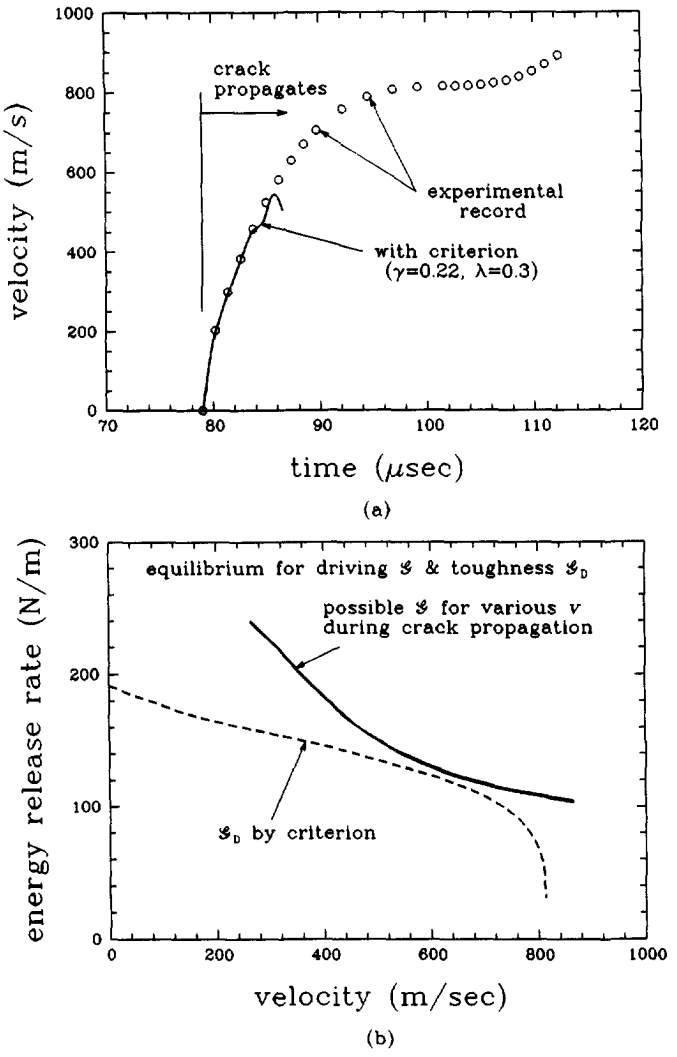

Fig. 6. (a) The resulting crack tip velocity after the initiation for the fracture criterion. The experimental record is shown with circles. (b) Energy release rate and crack tip velocity plot is used to illustrate why there is no converged solution for v.

crack tip speed. The resulting crack tip history is shown in Fig. 6(a). It shows sufficiently close agreement with the input velocity result, and demonstrates the usefulness of our fracture criterion and the iterative method. However, the computation with the criterion ends near $t = 86\ \mu$s due to there being no converged solution for v. This occurs not because of the computational error but because of the nature of the criterion curve. In order to obtain v, the equilibrium $\mathcal{G}_D = \mathcal{G}$ must exist for some v. Because the criterion curve is a decreasing function of v, it may not always intersect with the locus of possible $\mathcal{G}$ for various v as shown in Fig. 6(b). When this happens, there is no convergence. Thus, it is not attributed to the computational error but it occurs because of the slight difference between the model and the actual toughness condition.

Figure 7 shows the dynamic toughness surface of the PMMA–steel interface. Since the toughness formula (13) is expressed as a function of v and ψ, one can create a toughness surface for the dynamic interface crack for a given set of λ and γ. Such a surface is shown for $\lambda = 0.3$ and $\gamma = 0.22$ in Fig. 7. If this were a correct criterion, the energy release rate for a given crack tip velocity and phase angle must always lie on this surface for any crack propagation to occur. In fact, the path history of the propagating crack simulated here is shown with dark circles in the figure. Each circle represents a propagation through an element length. This plot clearly illustrates, starting from initiation at $v = 0$, how the crack tip accelerates causing the energy release rate to decrease.

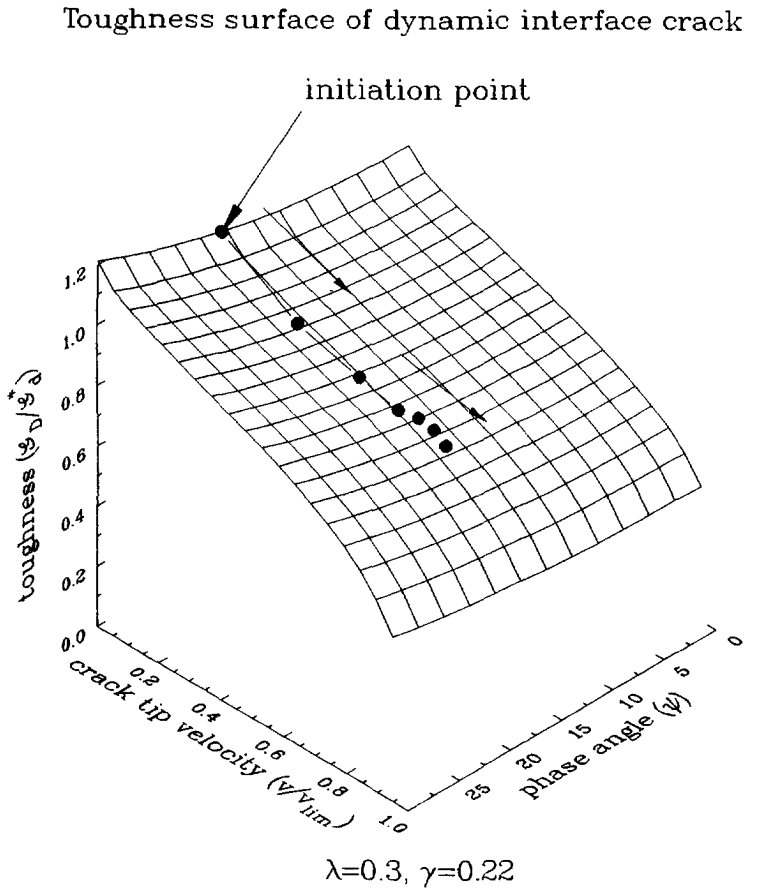

Fig. 7. Toughness surface of dynamic interface crack defined by ψ and v space given in eqn (13) for $\lambda = 0.3$ and $\gamma = 0.22$. The path taken by the propagating crack in the simulation is shown on the surface.

4. INTERLAMINAR DELAMINATION IN A COMPOSITE PANEL

4.1. *Computational model*

In the second part of our study, the computational procedures are modified and the interplay between an embedded delamination and a particular structural deformation mode is investigated. We consider a thin composite panel consisting of four differently oriented orthotropic laminae. Its cross-section is shown in Fig. 8. It is assumed that the panel contains a finite length interlaminar delamination and the generalized plane strain condition exists in the thickness direction. The location of the delamination is chosen to be between the third and fourth layers from the top and at the center of the panel. Each laminate has identical material properties which are supposed to represent epoxy-based laminae reinforced by unidirectional graphite fibers. They are $E_L = 103$ GPa, $E_T = 6$ GPa, $G_{TT} = 53$ GPa, $G_{LT} = 103$ GPa, $\nu_{LT} = 0.3$ and $\rho = 138$ kg m^{-3}, where the fiber direction is denoted by the subscript "L". The orientations of laminates are [0/90/90/0] where 0° is the direction

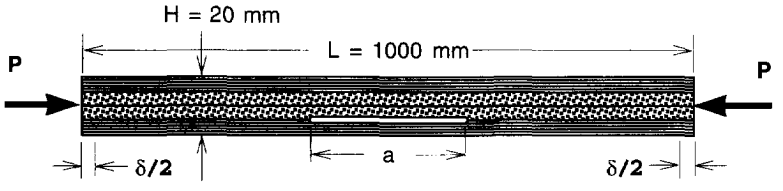

Fig. 8. Schematic of a composite panel consisting of four orthotropic laminae. The orientations of the laminae are [0/90/90/0]. The panel contains an embedded delamination between the third and fourth layers and is subjected to a large compressive load.

of the panel. The panel is subjected to a large compressive load parallel to its surfaces. The geometrical dimensions of the panel are $L = 1$ m and $H = 0.02$ m. The generalized plane strain condition also assumes the thickness to be $t = 1$ m.

The model possesses a symmetrical condition across the mid-section and only a half-model is used in the analysis. We have constructed finite element meshes for panels containing different crack lengths using 5000–6000 four-noded generalized plane strain elements. Since the panel is loaded to the post-buckling regime, large deformation finite element analysis is employed. However, throughout the calculations, strains are expected to remain relatively small while rotations can be large. The energy release rate and the stress intensity factors are computed by procedures similar to the previous analysis except with the following modifications. First the current direction of the crack tip is determined from the upper and lower crack planes near the tip and it is taken as the x_1-direction. All the field quantities in eqns (8) and (11) are transformed according to this local coordinate at every time step. This could be interpreted as corotational formulation of the crack tip analysis. Also a lateral deformation due to the generalized strain condition is taken into account in the calculations. In computations of I [eqn (11)], the asymptotic singular field for orthotropic materials is used for the auxiliary functions.

4.2. *Static results*

In order to determine the effect of an embedded delamination on the overall deformation mode of the panel, we initially carried out static analysis. Several models with various embedded crack lengths were considered. Since the deformation mode can be unstable, loading is simulated by end shortening. The equivalent end force is determined from the reaction force at the displaced node. In addition, a very small geometrical perturbation is applied in the undeformed configuration to trigger buckling. The shape of this perturbation is defined from the linearized buckling problem. To ensure accuracy, the critical buckling load of the perfect structure is calculated by a separate eigenvalue analysis and the result is compared with the critical load obtained from the load–deflection curve of the imperfect model. For each model, the difference between the two is negligible.

The resulting force and deflection relationships for various crack lengths are shown in Fig. 9. Here the analysis is carried out without any crack extension. The figure shows decreasing critical buckling load P_{cr} for increasing embedded crack length. Analyses have been performed for the cases with $a/L \leqslant 0.2$, and the results are identical to the "no crack" result. In the post-buckling regime, "unstable" behavior is observed for panels with crack length $0.3 \leqslant a/L \leqslant 0.7$. The unstable post-buckling behavior is produced by the coupling of two buckling modes. One is characterized by the overall panel buckling and the other is dominated by a local ligament buckling near the embedded delamination. Thus, a limit

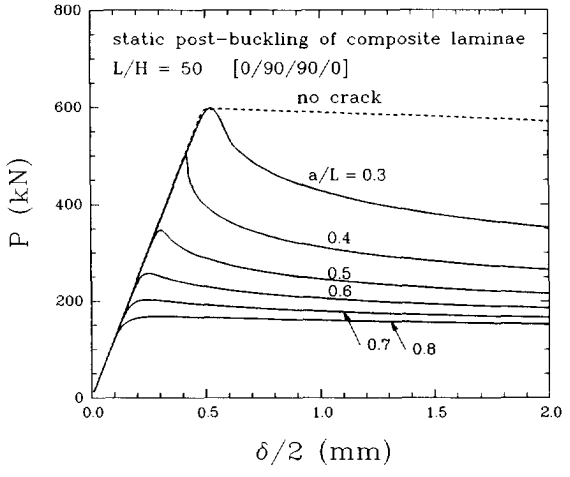

Fig. 9. Static load–deflection curves of the panels with various crack lengths. Unstable post-buckling behavior is observed for $0.3 \leqslant a/L \leqslant 0.7$.

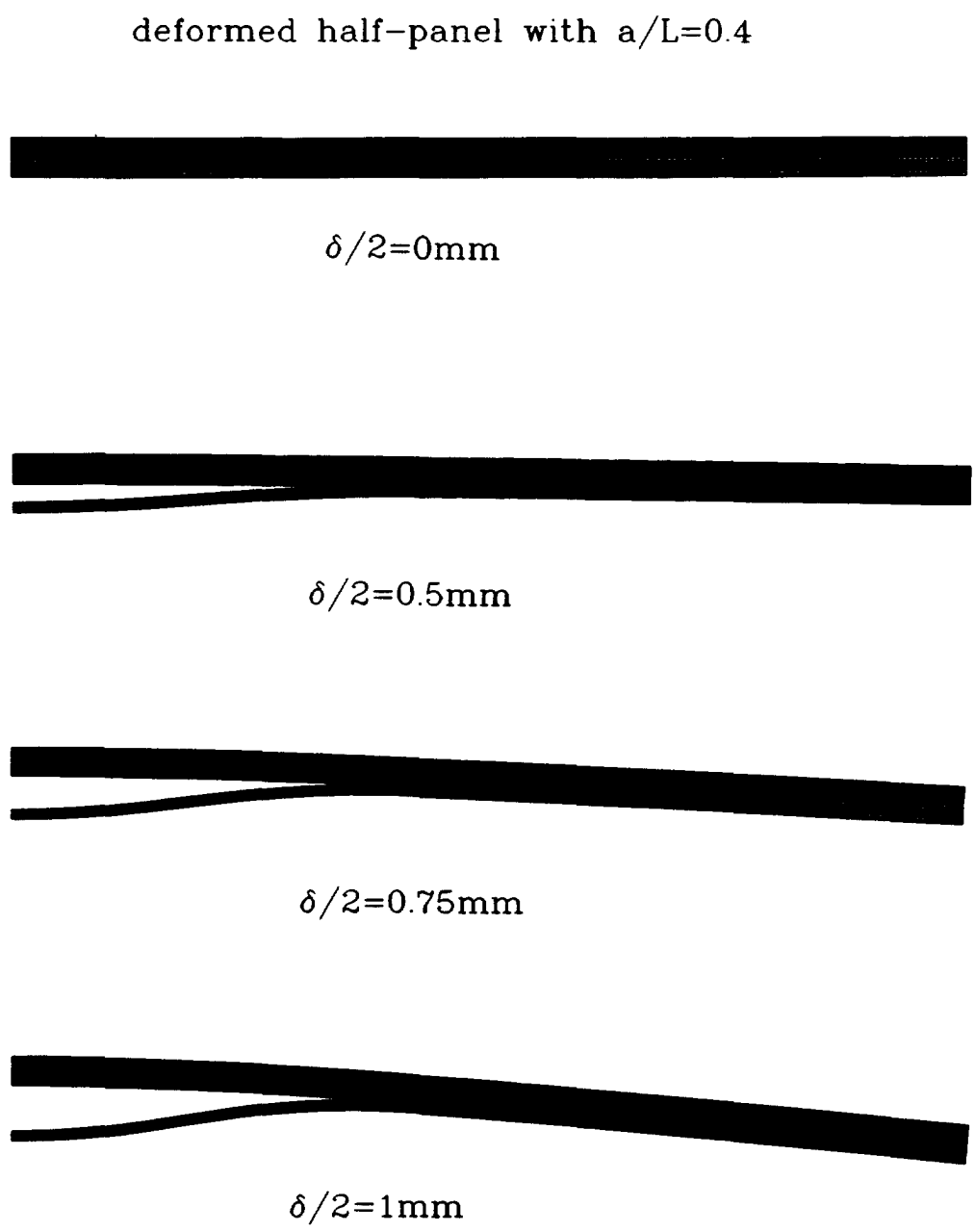

Fig. 10. Deformed finite element meshes of the panel with $a/L = 0.4$. Progression of two modes of buckling, overall panel and local ligament, can be observed.

load type behavior may occur when the panel contains sufficiently long embedded delamination. For $a/L \leqslant 0.2$, there is no local buckling of the ligament. Also for a very long delamination with $a/L \geqslant 0.8$, there is no coupling to the two buckling modes because each buckles as an independent panel. Figure 10 shows the progressing deformation of the $a/L = 0.4$ model. It clearly indicates the increasing crack opening and the overall and local buckling modes.

Using the modified domain integral formulation, the energy release rate computed for the various models with different crack lengths is shown in Fig. 11(a). For deflections less than that critical for buckling, there is hardly any crack opening and $\mathcal{G}$ remains near zero. Once buckling begins (e.g. $\delta/2 > 0.55$ mm for $a/L = 0.3$), the energy release rate rapidly increases. It is also seen that the rate of increase is larger for models with greater unstable post-buckling behavior (see Fig. 9). In fact, the model with $a/L = 0.3$ has the largest $\mathcal{G}$ for $\delta/2 > 0.65$ mm because of larger local ligament buckling near the crack. The mixed-mode

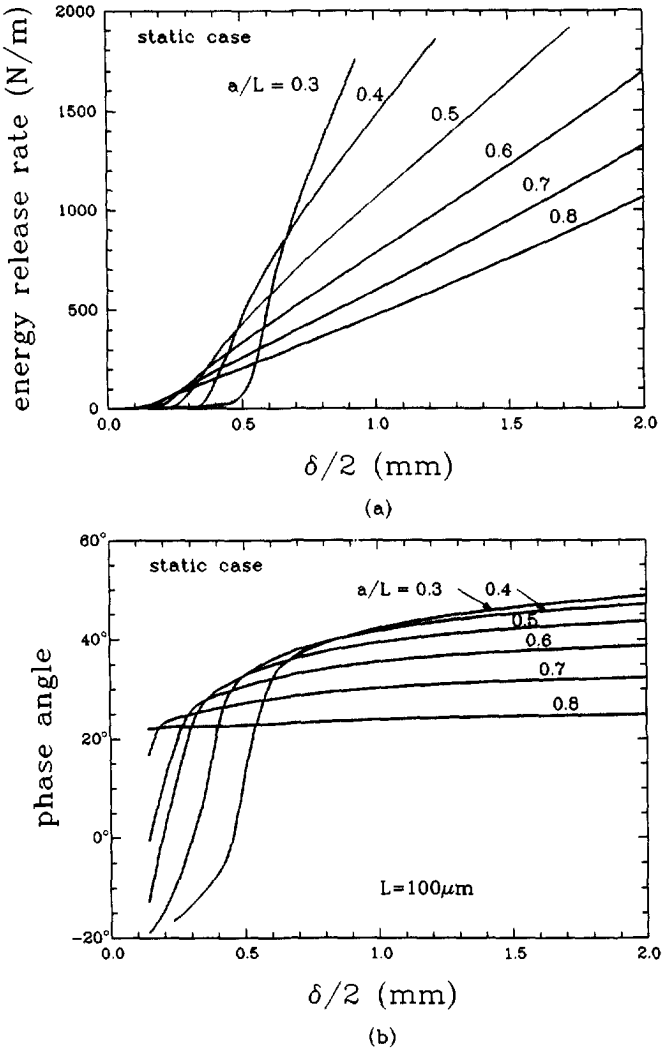

Fig. 11. Fracture parameters for various crack lengths are shown for the static case (a) energy release rate and (b) phase angle.

stress intensity factors are also calculated from the modified interaction integral (11). The phase angle with $L = 100\ \mu$m is shown on Fig. 11(b). The non-linear behavior of the phase angle is explained by the finite deformation of the panel. For all the cases, the phase angle increases with larger buckling mode displacements. The rate of increase is also greater for the models with shorter crack lengths.

4.3. *Dynamic results*

The results presented in the static case suggest a possible unstable delamination growth in the post-buckling regime. Here we simulate the dynamic propagation of an interlaminar crack in the composite plate. Since there is virtually no available experimental data for this problem and our present aim is to determine the applicability of the computational procedures, we adopt a simplified condition for the toughness criterion. It is assumed that the dynamic fracture toughness of the interface is expressed by a fraction of initiation toughness as

$$\mathcal{G}_D = 0.8\,\mathcal{G}_d. \tag{14}$$

Here $\mathcal{G}_d$ is the initiation toughness and the choice of 0.8 is arbitrary. This criterion ignores any effects of the crack tip velocity and the phase angle. It is similar to the bluntness

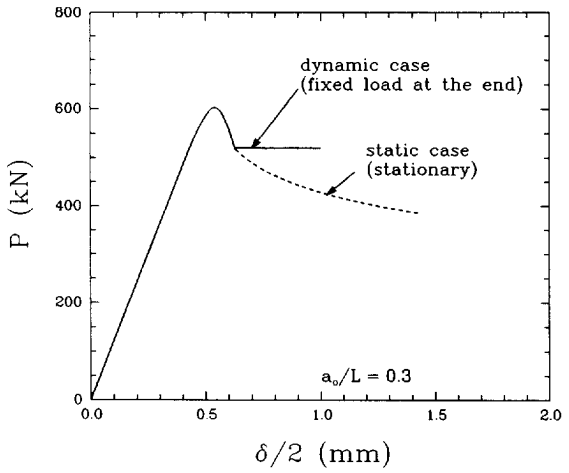

Fig. 12. Load–deflection curve used to illustrate the boundary condition for the dynamic case.

parameter criterion used by Freund (1990). Based on the static results, the initial crack length is chosen to be $a_0/L = 0.3$ and the initiation toughness is taken as $\mathcal{G}_d = 720$ N m^{-1}. The panel is gradually loaded by the prescribed displacement and once $\mathcal{G}$ reaches the initiation toughness, the end boundary condition is replaced with a fixed force $P = 520$ kN as shown in Fig. 12. This occurs just beyond the start of buckling. At this point, the dynamic toughness is set at $\mathcal{G}_D = 576$ N m^{-1} and the suitable crack tip velocity which results in the equivalent $\mathcal{G}$ is sought using the iterative procedure. The determination of the optimum velocity takes about five iterations for each node release. The increasing $\mathcal{G}$ during the stationary phase and the constant $\mathcal{G}$ during the propagating phase are shown in Fig. 13(a). The computational is carried out for 70 μs or a crack extension of $\Delta a = 0.5$ mm after the crack growth initiation. The phase angle during propagation is also computed and shown in Fig. 13(b). The result shows a very small decrease in ψ during the calculation. It is consistent with the static case where a small difference in ψ between $a/L = 0.3$ and 0.4 is observed in the post-buckling regime as shown in Fig. 10(b).

The computed crack tip velocity is shown in Fig. 14. To account for a sudden decrease of toughness, the velocity increases immediately after the initiation. After several microseconds, the velocity varies in the range $0 < v < 100$ m s^{-1}. The velocity increase near $t = 50$ μs is attributed to the unloading wave returning from the end. If the crack tip velocity remains in this range, a complete separation of the bottom laminate from the rest of the panel can occur in a few milliseconds.

5. DISCUSSION

In this work, the dynamic propagation of an interface crack is analyzed with emphasis placed on the determination of the fracture criterion and the implementation of the computational procedure to a complex structural problem. In the first part of the analysis, the interface crack between PMMA and steel is modeled based on the experiment by Lambros and Rosakis (1995) and the relevant fracture parameters are computed. We have observed two significant results for the dynamic interface crack and they are not consistent with the usual homogeneous crack results. One result is the crack tip speed approaching near or beyond the wave speed of the slower material. This occurs without the crack branching seen in homogeneous crack cases. The other is the decreasing energy release rate for a higher crack tip speed. Although explanations based on physical mechanisms are unclear, it appears the high crack tip speed is the result of the relatively weak interface and the large separation force supplied from the steel side.

In addition, there is a question as to whether crack propagation is controlled by the dynamic interface K-field in the real specimen. It is known that the condition for the existence of the K-field is more severe for the interface crack, especially under high crack

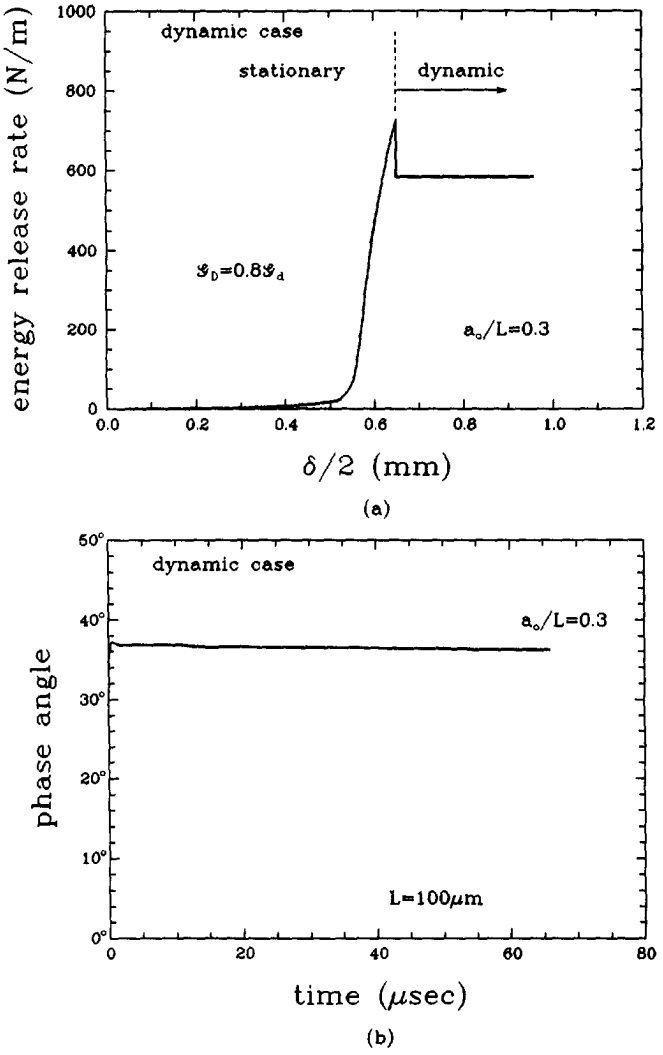

Fig. 13. (a) Energy release rate during stationary and propagation phases. The crack growth initiation begins when $\mathcal{G}_d$ = 720 N m^{-1} and the propagating toughness is set constant at $\mathcal{G}_D$ = 576 N m^{-1}. (b) Computed phase angle is shown as a function of elapsed time.

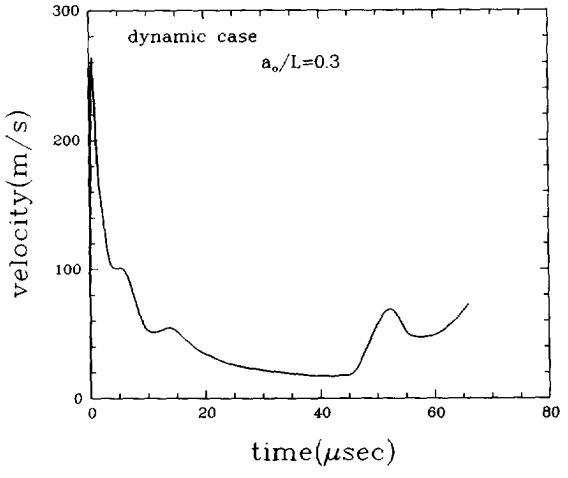

Fig. 14. The resulting crack tip velocity for the dynamic case. The crack propagates with constant toughness.

tip speeds as discussed by Liu *et al.* (1994). The requirement for K dominance is that a plane stress K-field exists outside the near tip three-dimensional region. Since the size of the near tip three-dimensional region, excluding the bimaterial boundary, grows while the size of K-field shrinks under higher velocity, it is likely that there is no distinct K-field when v is near the wave speed. Thus for the dynamic interface crack, it may be more useful to treat $\mathcal{G}_D$ as the critical value of energy flow rate instead of the magnitude of near tip field. Such an interpretation should still enable us to establish a fracture criterion based on energy release rate. Because it is useful for the interpretation of experimental data and also necessary for carrying out computational simulations of complex structures, we attempted to formulate a suitable criterion. Our formula takes into account the effects of phase angle and crack tip velocity. Determinations of optimum values for the parameters in the criterion must rely on experimental investigations such as the one carried out by Lambros and Rosakis (1995). They have also suggested a criterion based on fixed CTODs and showed a good agreement with their experimental record. Formulation and determination of an "ideal" criterion requires several experimental and numerical analyses. Features for an ideal criterion are, fewer parameters and a wide range of applicability both in terms of various interfaces and loading conditions.

In the second part of the our study, the computational procedures developed for the isotropic bimaterials are extended to orthotropic materials. In addition, more complex boundary conditions and geometry are considered. The interface fracture analysis is carried out for a composite panel containing a delamination and made of four differently oriented laminae. From the results of static analysis under large deformation, an important structural deformation mode is observed. When the panel contains an embedded delamination and is under large compressive load, a coupling of the global panel buckling and the local ligament buckling produces "unstable" post-buckling behavior. Such a condition is potentially hazardous for the integrity of structures. The energy release rate of the embedded delamination also increases rapidly during the unstable post-buckling phase. Motivated by this condition, we have simulated the dynamic crack propagation of the interlaminar delamination. Lacking any experimental data, we employed a simplified toughness condition and the iterative method to propagate the crack without prior input of the crack tip velocity history. The computed results show that the crack propagation occurs without a large variation in mode mixity. Based on the result for crack tip velocity, one can predict a total time for complete separation to be a few milliseconds. The successful implementation of the crack propagation simulation shows the ability to analyze failure modes of other structural models such as cylindrical vessels under large external pressure and panels under biaxial and shear loadings.

Acknowledgements—The authors gratefully acknowledge the support of ONR under grant No. N0001491J1352. Computations were performed on DEC AXP300. The finite element analysis was carried out with the ABAQUS code, which was made available under academic licence from Hibbitt, Karlson and Sorenson, Inc. Providence, Rhode Island.

REFERENCES

Freund, L. B. (1990). *Dynamic Fracture Mechanics*. Cambridge University Press, Cambridge.

Hutchinson, J. W. and Suo, Z. (1991). Mixed mode cracking in layered materials. In *Advance in Applied Mechanics* (Edited by J. W. Hutchinson and T. Y. Wu), Vol. 29, pp. 63–191. Academic Press, New York.

Kobayashi, T. and Dally, J. W. (1979). Dynamic photoelastic determination of the $\dot{a}$–K relation for 4340 steel. *ASTM STP* **711**, 189–210.

Lambros, J. and Rosakis, A. J. (1995). Dynamic decohesion of bimaterials: experimental observations and failure criteria. *Int. J. Solids Structures* **32**, 2677–2702.

Lo, C. Y., Nakamura, T. and Kushner, A. (1994). Computational analysis of dynamic crack propagation along bimaterial interface. *Int. J. Solids Structures* **31**, 145–168.

Liu, C., Lambros, J. and Rosakis, A. J. (1993). Highly transient elastodynamic crack growth in a bimaterial interface: higher order asymptotic analysis and experiment. *J. Mech. Phys Solids* **41**, 1887–1954.

Ravi-Chandar, K. and Knauss, W. G. (1984). An experimental investigation into dynamic fracture: III. On steady state crack propagation and crack branching. *Int. J. Fracture* **26**, 141–154.

Rosakis, A. J., Duffy, J. and Freund, L. B. (1984). The determination of dynamic fracture toughness of AISI 4340 steel by the shadow spot method. *J. Mech. Phys. Solids* **32**, 443–460.

Stroh, A. N. (1962). Steady state problems in anisotropic elasticity. *J. Math. Phys.* **41**, 77–103.

Tippur, H. V. and Rosakis, A. J. (1991). Quasi-state and dynamic crack growth along bimaterial interfaces: a note on crack tip field measurements using coherent gradient sensing. *Exp. Mech.* **31,** 243–251.
Willis, J. R. (1971). Fracture mechanics of interfacial cracks. *J. Mech. Phys. Solids* **19,** 353–368.
Wu, K. C. (1991). Explicit crack tip fields of an extending interface crack in an anisotropic bimaterial. *Int. J. Solids Structures* **27,** 455–466.
Yang, W., Suo, Z. and Shih, C. F. (1991). Mechanics of dynamic debonding. *Proc. R. Soc.* **433,** 679–697.